



Manuscript received 20 August 2019
Revised manuscript received 23 October 2019
Manuscript accepted 9 November 2019

© 2019 Geological Society of America. For permission to copy, contact editing@geosociety.org.

Magma accumulation beneath Santorini volcano, Greece, from P-wave tomography

B.G. McVey¹, E.E.E. Hooft¹, B.A. Heath¹, D.R. Toomey¹, M. Paulatto², J.V. Morgan², P. Nomikou³ and C.B. Papazachos⁴

- ¹Department of Earth Sciences, University of Oregon, Eugene, Oregon 97403, USA ²Department of Earth Science and Engineering, Imperial College London, London SW7 2AZ, UK
- ³Department of Geology and Geoenvironment, National and Kapodistrian University of Athens, Athens 157 72, Greece
- ⁴Geophysical Laboratory, Aristotle University of Thessaloniki, Thessaloniki 541 24, Greece

ABSTRACT

Despite multidisciplinary evidence for crustal magma accumulation below Santorini volcano, Greece, the structure and melt content of the shallow magmatic system remain poorly constrained. We use three-dimensional (3-D) velocity models from tomographic inversions of active-source seismic P-wave travel times to identify a pronounced low-velocity anomaly (-21%) from 2.8 km to 5 km depth localized below the northern caldera basin. This anomaly is consistent with depth estimates of pre-eruptive storage and a recent inflation episode, supporting the interpretation of a shallow magma body that causes seismic attenuation and ray bending. A suite of synthetic tests shows that the geometry is well recovered while a range of melt contents (4%-13%) to fully molten are allowable. A thin mush region (2%-7%) to 3%-10% melt) extends from the main magma body toward the northeast, observed as low velocities confined by tectono-magmatic lineaments. This anomaly terminates northwest of Kolumbo; little to no melt underlies the seamount from 3 to 5 km depth. These structural constraints suggest that crustal extension and edifice loads control the geometry of magma accumulation and emphasize that the shallow crust remains conducive to melt storage shortly after a caldera-forming eruption.

INTRODUCTION

After a caldera-forming eruption, the shallow magmatic system is rejuvenated by fresh injections of melt from the lower crust. Some studies suggest that shallow melt accumulates where crustal stresses are least compressive due to topographic loads and regional tectonic extension (Corbi et al., 2015). How quickly the magmatic system reforms, in what way the melt accumulates, and how long shallow melt is maintained in the upper crust are still debated (Cooper and Kent, 2014; Barboni et al., 2016; Cashman et al., 2017; Rubin et al., 2017).

Santorini, Greece, is an ideal volcano to address competing ideas of shallow magma storage because its geologic and historic eruption history is well studied and it currently maintains a shallow magma body which has sourced small eruptions following a recent caldera collapse. Santorini is a semi-submerged volcano in the Hellenic volcanic arc that has a history

of at least nine Plinian eruptions separated by inter-Plinian periods of frequent, effusive shieldbuilding events (Druitt et al., 1999). The Late Bronze Age (LBA or Minoan) eruption in 1630 BCE was the most recent caldera-forming eruption, of ~60-70 km³ dense-rock equivalent of magma (Johnston et al., 2014; Karátson et al., 2018). Subsequent effusive activity has formed the 400-m-tall Kameni shield islands within Santorini caldera, totaling ~3.2 km³ since 197 BCE, and most recently erupting in 1950 CE (Nomikou et al., 2014). From 2011 to 2012, Santorini experienced an unrest period including ground deformation measured by InSAR and GPS that was modeled to suggest 0.01-0.02 km³ of inflation between 4 and 5 km depth northwest of the Kameni islands (Parks et al., 2015). This inflation was attributed to an intrusion of melt that pooled at the same depth as that constrained for pre-eruptive storage of Kameni island lavas by a melt inclusion study (Druitt et al., 2016).

There is multi-disciplinary evidence for shallow magma accumulation below Santorini, but to date, no clear structural constraint on the magmatic system. In 2015, the PROTEUS (Plumbing Reservoirs of the Earth under Santorini) experiment collected dense seismic data using ~150 seismometers and ~14,000 controlled marine sources (Fig. 1) to image the magmatic system beneath Santorini. Data from the experiment revealed a low-velocity body below the northern caldera basin centered at 1.6 km depth, attributed to a high-porosity column created by collapse of a limited area of the caldera floor (Hooft et al., 2019). The longer-offset data in the present study deepen model coverage to 6 km to investigate the volume, geometry, and minimum melt content of shallow magma storage below Santorini. By combining geologic observations and tomographic images, we obtain a better understanding of both the nature of shallow reservoirs at active caldera-forming arc volcanoes during shield-building periods and the processes that influence the restructuring of the magmatic system.

TRAVEL-TIME TOMOGRAPHY

To image the structure of the caldera to ~6 km depth, we added ~30,000 longer-offset crustal-refraction, Pg, arrival picks that cross the caldera to the existing ~200,000 Pg picks of Heath et al. (2019) (see the GSA Data Repository¹). Seismic waves that travel below the northern caldera basin are attenuated with delayed arrivals—as expected for magma bodies (Lees, 2007). We used azimuthal swaths to enhance lateral continuity for rays passing through the magmatic system (Fig. 2). To improve our ability to pick the attenuated caldera-crossing data, we stacked

CITATION: McVey, B.G., et al., 2020, Magma accumulation beneath Santorini volcano, Greece, from P-wave tomography: Geology, v. 48, p. doi.org/10.1130/G47127.1

, https://

¹GSA Data Repository item 2020061, descriptions and illustrations of the seismic data analysis, tomographic inversion, physical property analysis, synthetic tomographic modeling, and volume calculation, is available online at http://www.geosociety.org/datarepository/2020/, or on request from editing@geosociety.org.

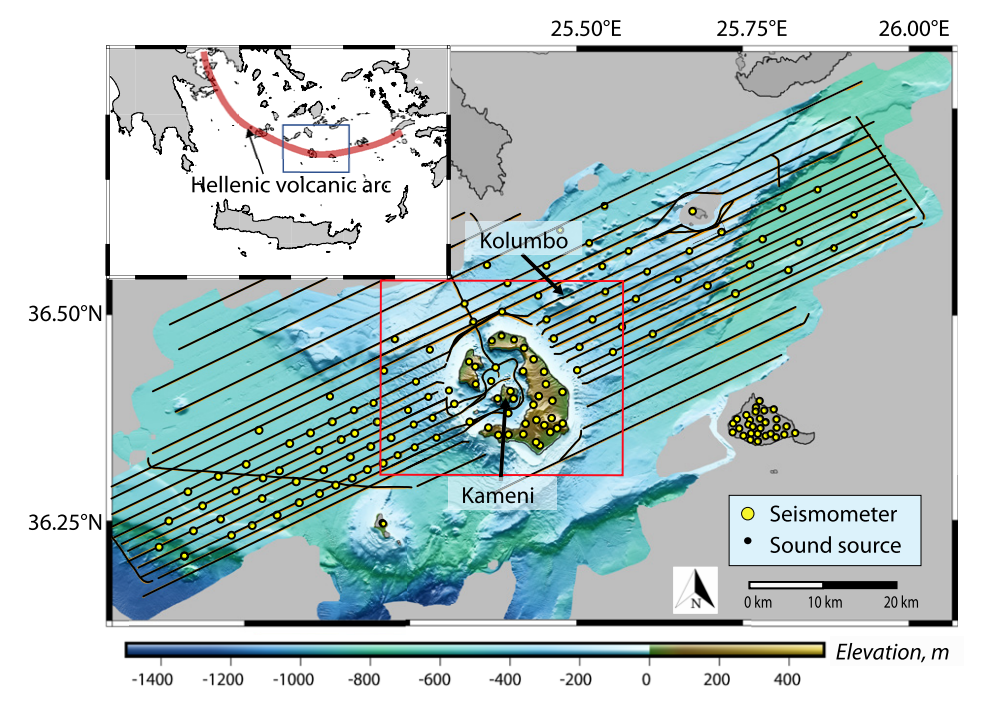


Figure 1. Map of area of PROTEUS (Plumbing Reservoirs of the Earth under Santorini) experiment, Santorini volcano, Greece, showing bathymetry (Nomikou et al., 2012; Hooft et al., 2017) and seismic experiment geometry (Heath et al., 2019). Seismic recorders (in yellow) include ocean bottom seismometers (OBS) and land stations. Shot lines of seismic sources (in black) were generated from airguns on the R/V Marcus G. Langseth. Area of this study is within the red square. Inset map indicates regional geography and volcanic arc.

the hydrophone and vertical components of the seismometer and used a low-frequency bandpass filter (Fig. DR1 in the Data Repository).

We used a seismic tomography method to invert first-arriving P-wave traveltimes for a three-dimensional (3-D) velocity model (Toomey et al., 1994) (see the Data Repository). Bathymetry was explicitly included, and the magnitude and roughness of model perturbations were penalized. We followed the parameterization of

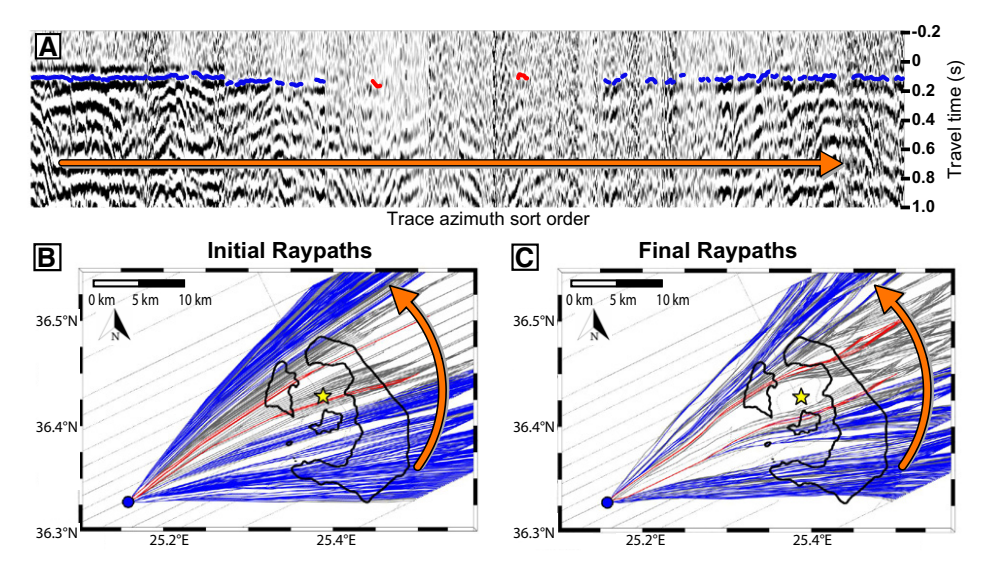


Figure 2. Seismic data and ray coverage, Santorini volcano, Greece. (A) Azimuthal seismic data recorded at one station, flattened on predicted arrivals through the final velocity model. Data are stack of hydrophone and vertical channels, filtered from 4 to 12 Hz (Fig. DR1 in the Data Repository [see footnote 1]). Traveltime picks are shown in blue and red. Red traveltime picks are within the attenuated zone. Orange arrow shows azimuth for each record increasing from south to north. (B) Raypaths associated with azimuthal seismic data, probing the initial model, colored to match traveltime picks. Gray raypaths have no traveltime pick. Initial ray coverage is evenly distributed. (C) Same raypaths as in B, now probing the final model. Rays within the attenuated zone, in red, bend around the low-velocity volume in the northern caldera basin centered at the location of recent inflation (star; Parks et al., 2015).

Heath et al. (2019) and presented a $28 \times 33 \times 6$ km subset of the full velocity model, which has a root-mean-squared misfit of 15.5 ms. The derivative weight sum (Toomey et al., 1990) and checkerboard tests (Figs. DR5–DR6) show ray coverage to 5.5–6 km depth and recovery of features with dimensions $3 \times 3 \times 1$ km to 4 km depth and with dimensions of $5 \times 5 \times 2$ km to 5 km depth.

RESULTS

The traveltime data added in this study deepen the model coverage (Fig. 3), revealing a low-velocity volume centered below the northern caldera basin (caldera low-velocity volume; CLV) with a limb that extends ~15 km northeastward (linear low-velocity volume; LLV). Ray bending provides direct evidence for the CLV. We simplify the wavefront, which has a finite sensitivity kernel, as a ray path that takes the fastest path from the airgun to the seismometer. Rays traveling through the starting model have evenly distributed paths between source and receiver with little bending (Fig. 2; Fig. DR2). As the inversion progresses through each iteration, the rays bend around a volume in the northern caldera basin, where geodetic models suggest the recent inflation was located (Parks et al., 2015)—clear evidence for a CLV in the northern part of the caldera. However, because very few rays probe the CLV in the final model, the recovered velocity image provides only the minimum perturbation required to exclude rays.

The CLV northwest of the Kameni islands is directly below the hypothesized caldera collapse column (Hooft et al., 2019) and has a maximum P-wave velocity anomaly of -21% at 3.4 km depth (Fig. DR3). This anomaly is of similar depth as, but of larger magnitude than, those associated with upper crustal magma storage at Mount St. Helens (Washington, USA), Newberry (Oregon, USA), Deception Island (South Shetland Islands, Antarctica), Montserrat (Lesser Antilles), and Avacha (Kamchatka Peninsula, Russia) (Kiser et al., 2018; Heath et al., 2015; Ben-Zvi et al., 2009; Paulatto et al., 2019, Bushenkova et al., 2019). Surrounding the CLV to the northwest and southeast are regions of high velocity (Fig. 3; Fig. DR3), similar to observations at these other arc volcanoes. The fast regions, composed of solidified intrusives or metamorphic rock, further enhance ray bending around the CLV.

We consider temperature and pressure conditions, magma composition, and pore-space geometry to estimate the melt fraction required by the tomographically recovered CLV (see the Data Repository). We use the self-consistent effective medium method to model interconnected melt in spheroids (Berryman, 1980). Pore aspect ratios from 0.05 to 0.5 represent melt distributions encompassing grain-boundary films, dikes, sills, and subspherical

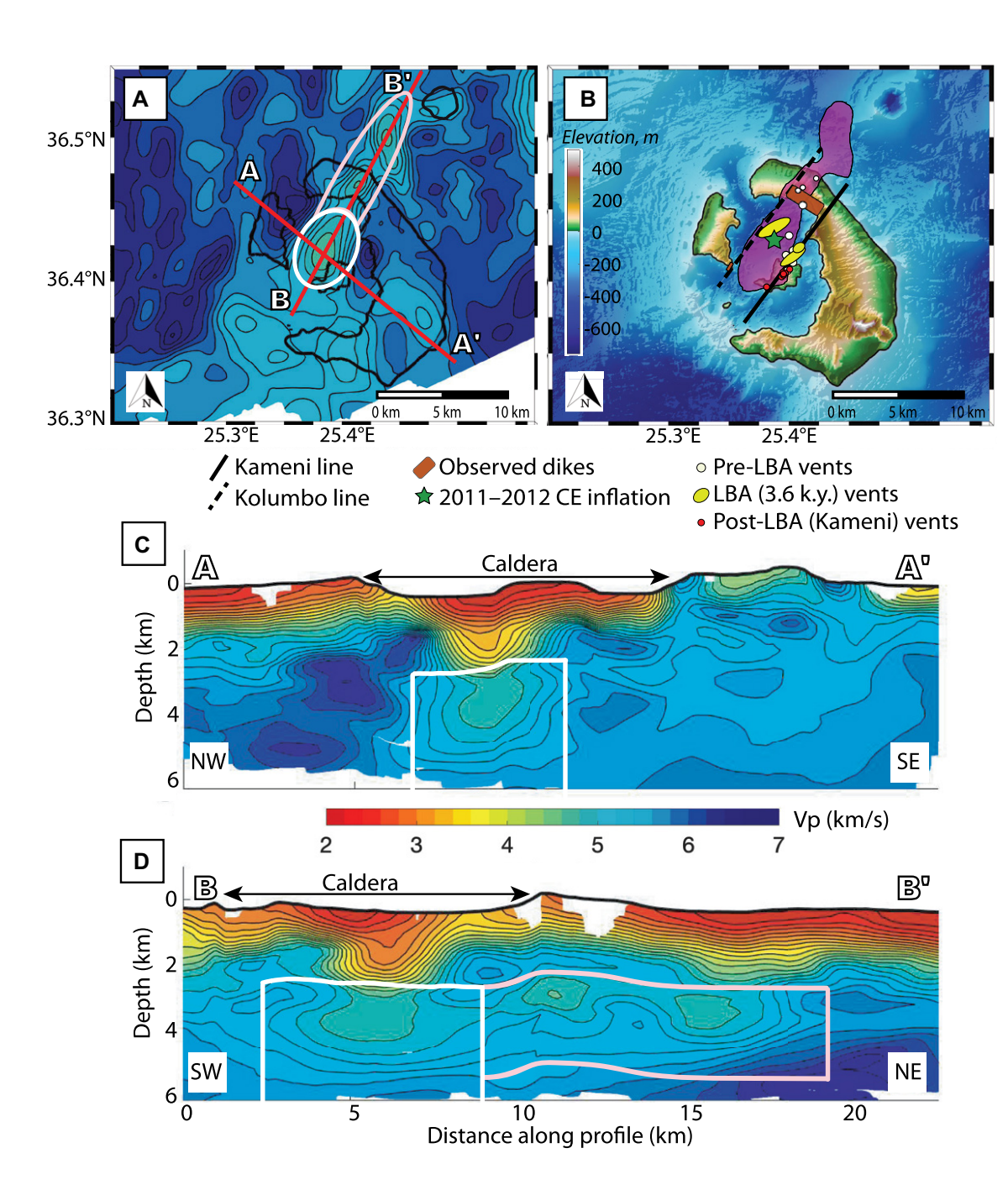


Figure 3. Tomographic P-wave velocity (Vp) model and geologic setting, Santorini volcano. Greece. (A) Depth slice at 3.4 km depth showing cross-section locations. (B) Bathymetry (Nomikou et al., 2012; Hooft et al., 2017) with the Kolumbo and Kameni lineaments defined by Heath et al. (2019). These lineaments bound the caldera lowvelocity volume (CLV) and linear low-velocity volume (LLV), indicated in purple using 5.3 km/s velocity contour, and are perpendicular to the regional extension direction. Dikes in the caldera walls that strike northeast-southwest (Browning et al., 2015), all vents for past 180 k.y. (Hooft et al., 2019; Druitt et al., 1999), and recent inflation (Parks et al., 2015) fall on, or within, these lineaments. LBA-Late Bronze Age (Minoan) eruption. (C) Cross section A-A' through the CLV. (D) Cross section B-B' through the LLV. All velocity panels use a contour interval of 0.2 km/s. Bounds of the synthetic CLV and LLV are outlined in white and pink. respectively (Fig. DR9 in the Data Repository [see footnote 1]). White regions of image mask inadequate initial ray coverage (Fig. DR5).

melt pockets. For the CLV, this range gives an average of 4%–13% melt from 2.8 to 5 km depth with a maximum of 6%–17% at 3.4 km (Fig. DR4). These melt fractions are the minimum values required by the tomographically recovered velocity image.

We use a suite of geologically motivated synthetic tests to further investigate how well the geometry, depth extent, and melt content of the magmatic system beneath Santorini are constrained (Figs. DR7–DR11). Because we under-recover low-velocity anomalies beneath the caldera, synthetics require a reduced velocity of at least 4 km/s (melt content of 11%–30%) within the CLV to reproduce the observed model. In addition, a fully molten body is tomographically resolved to have the same

velocity anomaly as the result. The map-view geometry is well resolved and well recovered. Tests of the depth extent of the low-velocity body show that we can exclude a melt accumulation that is thinner than what is recovered. Instead, melt must be present to at least 5 km depth. In fact, melt likely extends below 6 km depth, but insufficient deeper ray coverage limits the tomography model from requiring melt below 5 km.

The low-velocity region under Santorini is elongated ~15 km northeast-southwest (LLV), perpendicular to the regional extension direction, and has an average velocity anomaly of -14% (minimum melt fraction of 2%-7%). Synthetics show that two localized low-velocity concentrations within the LLV are an artifact of

the tomographic inversion; complex 3-D raypaths cause focusing of low velocities at these locations. However, the orientation and lateral extent of low velocities out of the caldera are robust, and synthetics require a small melt fraction (3%–10%). Notably, the LLV does not connect with Kolumbo seamount, where, at 3.4 km depth, velocities are somewhat reduced (5.4 km/s), consistent with little to no melt (0%–1%) (Fig. 3B).

We construct a final synthetic model that is consistent with geological models of magmatic systems and with our tomographic recovery tests (Fig. DR11). Beneath the northern caldera of Santorini, it includes a zone of partial melt (11%–30%) from 2.8 to 5 km depth underlain by a mush column (3%–10% melt) and a shallow

northeast-southwest linear elongation of mush (3%–10% melt from 2.8 to 5 km depth). This is our preferred interpretation (Fig. 4) and the recovered tomographic model reproduces the main features of the observed model well. The results support melt accumulation below the caldera with a higher melt content than along the LLV—a result that is consistent with pronounced seismic attenuation and ray bending primarily associated with the northern caldera.

DISCUSSION

We infer that the CLV under Santorini's northern caldera basin is the location of inter-caldera magma storage and the source of Kameni island eruptions since the LBA caldera-forming eruption ~3600 yr ago. The CLV is centered at the approximate depth and location of the 2011-2012 inflation source (Parks et al., 2015; Fig. 4) and offset from the Kameni islands. Its depth is also consistent with pre-eruptive storage of Kameni island dacites as determined from melt inclusions (Druitt et al., 2016). Rays that bend to avoid being slowed by the CLV are associated with the most heavily attenuated seismic data. The recovered CLV requires high temperatures and partial melt that absorbs energy from seismic waves that interact with it (Lees, 2007). Ray bending, seismic attenuation, and geodetic and petrologic observations consistently suggest that magma is currently stored in the upper crust below Santorini's northern caldera basin.

The volume of CLV that requires melt is $\sim 35 \pm 8$ km³ (see the Data Repository). We radially distribute the required melt content (maximum 13% at center) throughout the body

and find that at least 2.2 km³ (range 1.1–5.6 km³) of melt currently resides below the caldera. This is much larger than the volume of 0.01–0.02 km³ intruded from 2011 to 2012 (Parks et al., 2015) and is similar to the total volume of the Kameni islands (3.2 km³; Nomikou et al., 2014). Huijsmans et al. (1988) suggested that Kameni magma represents a new batch of melt from depth following the LBA eruption. Regardless of whether the shallow magma body contains unerupted LBA magmas or is completely composed of fresh Kameni magmas, a mush body containing at least ~2.2 km³ melt is observed just 3600 yr after catastrophic collapse and indicates the presence of long-lasting melt at shallow depths.

The LLV from Santorini toward Kolumbo supports a strong relationship between tectonism and magmatism. It is bounded by parallel, tomographically defined tectono-magmatic lineaments: the Kolumbo Line to the northwest, and the Kameni Line to the southeast (Heath et al., 2019; Fig. 3). These lineaments are subparallel to active northeast-southwest-trending regional faults and regional volcanic chains and vents (Nomikou et al., 2012). All eruptive vents of the last 180 k.y. are centered on, or between, these lineaments, as well as the dikes in the caldera walls (Fig. 3; Hooft et al., 2019; Druitt et al. 1999; Browning et al., 2015). A previous earthquake tomography study also recovered a linear low-velocity region elongated in this direction, but at greater depth (5-7 km), and attributed it to a tectonic zone that could provide pathways for ascending magma (Dimitriadis et al., 2010). In spite of the geometric alignment, we hesitate to attribute the LLV to a shallow magmatic connection between Santorini and Kolumbo because (1) it terminates short of, and slightly to the northwest of, Kolumbo, and (2) geochemical analysis of eruptive products from the two volcanoes indicate independent crustal differentiation (Klaver et al., 2016; Rizzo et al., 2016). A possible explanation for this feature is a zone of magmatic intrusions, similar to northeast-striking dikes in the caldera wall (Browning et al., 2015). It is also notable that recent volcanism at the Kameni islands and Kolumbo is consistently located on the southern boundary of the LLV.

The geometry of melt accumulation below Santorini suggests that the shallow structure is controlled by regional extension and topographic loads. The main magma body is located within the caldera, directly below a low-density volume, where unloading may rotate least compressive stresses to vertical (Corbi et al., 2015). The combination of topographic caldera rim loads and localized unloading could promote post-caldera magma accumulation under the northern caldera basin (Hooft et al., 2019). While these localized top-down controls concentrate most melt under the caldera, regional extensional stresses also promote magma accumulation in the northeast-southwest direction. Associated tectono-magmatic lineaments provide pathways for melt to migrate to the surface, localizing past eruption centers (Fig. 3).

CONCLUSION

At Santorini, we used a high-density seismic experiment and extensive synthetic testing to image a 35 ± 8 km³ low-velocity volume. We recover a significant velocity reduction of -21% at 3.4 km depth, consistent with preeruptive storage of Kameni island lavas since the LBA eruption ~3600 yr ago. Synthetic tests, ray bending, and seismic attenuation show that melt is most concentrated under the northern caldera basin, with an inferred melt content ranging from 4%–13% to fully molten. Magma accumulation extends from the main body, with decreased melt content (minimum 2%–7%, maximum 3%–10%), ~15 km northeastward (Fig. 4), terminating to the northwest of Kolumbo seamount. The main body and mush zone are bounded by tectono-magmatic lineaments, which provide pathways for melt to reach the surface. This shallow structure has likely prevailed through multiple eruption cycles because (1) extensional fracturing of the crust has persistently focused magmatism between tectono-magmatic lineaments, and (2) edifice stresses generated by low-density collapse and caldera topography have repeatedly focused inter-caldera pooling. The shallow magmatic system revealed in our study shows remarkable correlation with geodetic and petrologic investigations of Santorini and suggests that the shallow crust remains conducive to melt storage shortly after a caldera-forming eruption.

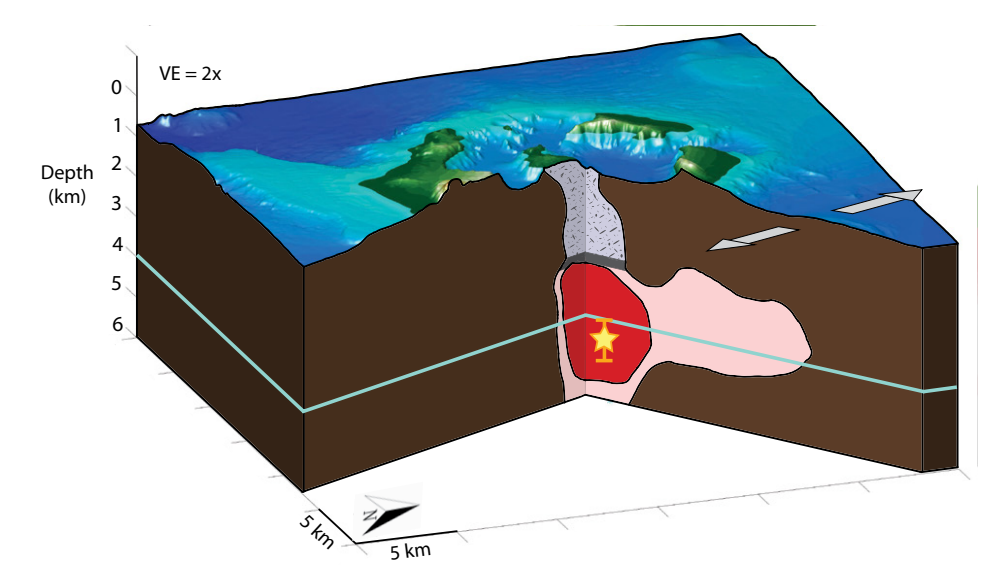


Figure 4. Conceptual model of the shallow magmatic structure of Santorini volcano, Greece, including pre-eruptive storage depth for Kameni island dacites (teal line at 4 km; Druitt et al., 2016) and point pressure source estimated from recent inflation (yellow star with error bars; Parks et al., 2015). Caldera low-velocity volume (red): melt accumulates below a high-porosity column formed during the caldera collapse (gray pattern), separated by a competent layer (Hooft et al., 2019). Linear low-velocity volume (pink): shallow mush region extends from the main body, perpendicular to the regional extension (gray arrows). VE—vertical exaggeration.

ACKNOWLEDGMENTS

For their roles in the data collection, we thank the officers, crew, and marine management office of the R/V Marcus G. Langseth, as well as the Ocean Bottom Seismograph Instrument Pool (OBSIP) personnel for help in the execution of this project. We also thank the personnel involved in the land station deployment and recovery. This work benefited from access to the University of Oregon (Eugene, Oregon, USA) high-performance computer, Talapas. Data used in this research were provided by instruments from the OBSIP (http://www.obsip.org), which is funded by the U.S. National Science Foundation (NSF). OBSIP data are archived at the IRIS Data Management Center (http://www.iris.edu). We thank Tim Druitt, Steven Sparks, Joseph Dufek, Paul Wallace, the entire PRO-TEUS science team, and two anonymous reviewers for helpful discussions and/or reviews. The experiment and analysis were supported by the NSF under grant OCE-1459794 to the University of Oregon and by Leverhulme grant RPG-2015-363 to Imperial College London.

REFERENCES CITED

- Barboni, M., Boehnke, P., Schmitt, A.K., Harrison, T.M., Shane, P., Bouvier, A.-S., and Baumgartner, L., 2016, Warm storage for arc magmas: Proceedings of the National Academy of Sciences of the United States of America, v. 113, p. 13,959–13,964, https://doi.org/10.1073/pnas.1616129113.
- Ben-Zvi, T., Wilcock, W.S.D., Barclay, A.H., Zandomeneghi, D., Ibáñez, J.M., and Almendros, J., 2009, The P-wave velocity structure of Deception Island, Antarctica, from two-dimensional seismic tomography: Journal of Volcanology and Geothermal Research, v. 180, p. 67–80, https://doi.org/10.1016/j.jvolgeores.2008.11.020.
- Berryman, J.G., 1980, Long-wavelength propagation in composite elastic media: II. Ellipsoidal inclusions: The Journal of the Acoustical Society of America, v. 68, p. 1820–1831, https://doi.org/10.1121/1.385172.
- Browning, J., Drymoni, K., and Gudmundsson, A., 2015, Forecasting magma-chamber rupture at Santorini volcano, Greece: Scientific Reports, v. 5, 15785, https://doi.org/10.1038/srep15785.
- Bushenkova, N., Koulakov, I., Senyukov, S., Gordeev, E.I., Huang, H.-H., El Khrepy, S., and Al Arifi, N., 2019, Tomographic images of magma chambers beneath the Avacha and Koryaksky volcanoes in Kamchatka: Journal of Geophysical Research: Solid Earth, v. 124, p. 9694–9713, https://doi.org/10.1029/2019JB017952.
- Cashman, K.V., Sparks, R.S.J., and Blundy, J.D., 2017, Vertically extensive and unstable magmatic systems: A unified view of igneous processes: Science, v. 355, eaag3055, https://doi .org/10.1126/science.aag3055.
- Cooper, K.M., and Kent, A.J.R., 2014, Rapid remobilization of magmatic crystals kept in cold storage: Nature, v. 506, p. 480–483, https://doi.org/10.1038/nature12991.
- Corbi, F., Rivalta, E., Pinel, V., Maccaferri, F., Bagnardi, M., and Acocella, V., 2015, How caldera collapse shapes the shallow emplacement and

- transfer of magma inactive volcanoes: Earth and Planetary Science Letters, v. 431, p. 287–293, https://doi.org/10.1016/j.epsl.2015.09.028.
- Dimitriadis, I., Papazachos, C., Panagiotopoulos, D., Hatzidimitriou, P., Bohnhoff, M., Rische, M., and Meier, T., 2010, P and S velocity structures of the Santorini-Coloumbo volcanic system (Aegean Sea, Greece) obtained by non-linear inversion of travel times and its tectonic implications: Journal of Volcanology and Geothermal Research, v. 195, p. 13–30, https://doi.org/10.1016/j.jvolgeores.2010.05.013.
- Druitt, T.H., Edwards, L., Mellors, R.M., Pyle, D.M., Sparks, R.S.J., Lanphere, M., Davies, M., and Barreirio, B., 1999, Santorini Volcano: Geological Society of London Memoir 19, 165 p.
- Druitt, T.H., Mercier, M., Florentin, L., Deloule, E., Cluzel, N., Flaherty, T., Médard, E., and Cadoux, A., 2016, Magma storage and extraction associated with Plinian and interplinian activity at Santorini caldera (Greece): Journal of Petrology, v. 57, p. 461–494, https://doi.org/10.1093/petrology/egw015.
- Heath, B.A., Hooft, E.E.E., Toomey, D.R., and Bezada, M.J., 2015, Imaging the magmatic system of Newberry Volcano using joint active source and teleseismic tomography: Geochemistry Geophysics Geosystems, v. 16, p. 4433–4448, https://doi.org/10.1002/2015GC006129.
- Heath, B.A., Hooft, E.E.E., Toomey, D.R., Papazachos, C.B., Nomikou, P., Paulatto, M., Morgan, J.V., and Warner, M.R., 2019, Tectonism and its relation to magmatism around Santorini volcano from upper crustal P-wave velocity: Journal of Geophysical Research: Solid Earth, https://doi.org/10.1029/2019JB017699.
- Hooft, E.E.E., et al., 2017, Backarc tectonism, volcanism, and mass wasting shape seafloor morphology in the Santorini-Christiana-Amorgos region of the Hellenic Volcanic Arc: Tectonophysics, v. 712–713, p. 396–414, https://doi.org/10.1016/j.tecto.2017.06.005.
- Hooft, E.E.E., Heath, B.A., Toomey, D.R., Paulatto, M., Papazachos, C.B., Nomikou, P., Morgan, J.V., and Warner, M.R., 2019, Seismic imaging of Santorini: Subsurface constraints on caldera collapse and present-day magma recharge: Earth and Planetary Science Letters, v. 514, p. 48–61, https://doi.org/10.1016/j. epsl.2019.02.033.
- Huijsmans, J.P.P., Barton, M., and Salters, V.J.M., 1988, Geochemistry and evolution of the calcalkaline volcanic complex of Santorini, Aegean Sea, Greece: Journal of Volcanology and Geothermal Research, v. 34, p. 283–306, https://doi .org/10.1016/0377-0273(88)90039-X.
- Johnston, E.N., Sparks, R.S.J., Phillips, J.C., and Carey, S., 2014, Revised estimates for the volume of the Late Bronze Age Minoan eruption, Santorini, Greece: Journal of the Geological Society, v. 171, p. 583–590, https://doi.org/10.1144/ jgs2013-113.
- Karátson, D., Gertisser, R., Telbisz, T., Vereb, V., Quidelleur, X., Druitt, T., Nomikou, P., and Kósik, S., 2018, Towards reconstruction of the lost Late Bronze Age intra-caldera island of

- Santorini, Greece: Scientific Reports, v. 8, 7026, https://doi.org/10.1038/s41598-018-25301-2.
- Kiser, E., Levander, A., Zelt, C., Schmandt, B., and Hansen, S., 2018, Focusing of melt near the top of the Mount St. Helens (USA) magma reservoir and its relationship to major volcanic eruptions: Geology, v. 46, p. 775–778, https://doi.org/10.1130/G45140.1.
- Klaver, M., Carey, S., Nomikou, P., Smet, I., Godelitsas, A., and Vroon, P., 2016, A distinct source and differentiation history for Kolumbo submarine volcano, Santorini volcanic field, Aegean arc: Geochemistry Geophysics Geosystems, v. 17, p. 3254–3273, https://doi .org/10.1002/2016GC006398.
- Lees, J.M., 2007, Seismic tomography of magmatic systems: Journal of Volcanology and Geothermal Research, v. 167, p. 37–56, https://doi.org/10.1016/j.jvolgeores.2007.06.008.
- Nomikou, P., Carey, S., Papanikolaou, D., Croff Bell, K., Sakellariou, D., Alexandri, M., and Bejelou, K., 2012, Submarine volcanoes of the Kolumbo volcanic zone NE of Santorini Caldera, Greece: Global and Planetary Change, v. 90–91, p. 135–151, https://doi.org/10.1016/j.gloplacha.2012.01.001.
- Nomikou, P., et al., 2014, The emergence and growth of a submarine volcano: The Kameni islands, Santorini (Greece): GeoResJ, v. 1–2, p. 8–18, https://doi.org/10.1016/j.grj.2014.02.002.
- Parks, M.M., et al., 2015, From quiescence to unrest: 20 years of satellite geodetic measurements at Santorini volcano, Greece: Journal of Geophysical Research: Solid Earth, v. 120, p. 1309–1328, https://doi.org/10.1002/2014JB011540.
- Paulatto, M., Moorkamp, M., Hautmann, S., Hooft, E., Morgan, J.V., and Sparks, R.S.J., 2019, Vertically extensive magma reservoir revealed from joint inversion and quantitative interpretation of seismic and gravity data: Journal of Geophysical Research: Solid Earth, https://doi .org/10.1029/2019JB018476.
- Rizzo, A.L., Caracausi, A., Chavagna, V., Nomikou, P., Polymenakou, P.N., Mandalakis, M., Kotoulas, G., Magoulas, A., Castillo, A., and Lampridou, D., 2016, Kolumbo submarine volcano (Greece): An active window into the Aegean subduction system: Scientific Reports, v. 6, 28013, https:// doi.org/10.1038/srep28013.
- Rubin, A.E., Cooper, K.M., Till, C.B., Kent, A.J.R., Costa, F., Bose, M., Gravley, D., Deering, C., and Cole, J., 2017, Rapid cooling and cold storage in silicic magma reservoir recorded in individual crystals: Science, v. 356, p. 1154–1156, https:// doi.org/10.1126/science.aam8720.
- Toomey, D.R., Purdy, G.M., Solomon, S.C., and Wilcock, W.S.D., 1990, The three-dimensional seismic velocity structure of the East Pacific Rise near latitude 9°30′N: Nature, v. 347, p. 639–645, https://doi.org/10.1038/347639a0.
- Toomey, D.R., Solomon, S.C., and Purdy, G.M., 1994, Tomographic imaging of the shallow crustal structure of the East Pacific Rise at 9°30′N: Journal of Geophysical Research, v. 99, p. 24,135–24,157, https://doi.org/10.1029/94JB01942.

Printed in USA